www.gi.sanu.ac.rs, www.doiserbia.nb.rs
J. Geogr. Inst. Cvijic. 2025, 75(2), pp. 233–250

Original scientific paper

UDC: 631.111.3(574)
https://doi.org/10.2298/IJGI2502233S

Received: March 31, 2025
Reviewed: May 14, 2025
Accepted: May 30, 2025

SOIL SALINIZATION AND ITS IMPACT ON THE DEGRADATION OF AGRICULTURAL LANDSCAPES OF THE TALAS DISTRICT, KAZAKHSTAN

Zhassulan Smanov[1], *Salavat Duisenbayev*[2], *Kanat Zulpykharov*[1,2], *Shakhislam Laiskhanov*[3], *Zhanarys Turymtayev*[1], *Zhenis Kozhayev*[4], *Emin Atasoy*[5], *Omirzhan Taukebayev*[1,6*]

[1]Al-Farabi Kazakh National University, Space Technologies and Remote Sensing Center, Almaty, Kazakhstan; e-mails: zhassulan.smanov1307@gmail.com; kanat.zulpykharov@gmail.com; zhanarys.turymtayev@kaznu.edu.kz; omirzhan.taukebayev@kaznu.edu.kz
[2]Al-Farabi Kazakh National University, Faculty of Geography and Environmental Sciences, Department of Geography, Land Management, and Cadastre, Almaty, Kazakhstan; e-mail: duysenbaev.s.m.64@gmail.com
[3]International Educational Corporation, Department of Science and Innovation, Almaty, Kazakhstan; e-mail: laiskhanov@gmail.com
[4]Satbayev University, O. Baikonyrov Institute of Mining and Metallurgical, Department of Surveying and Geodesy, Almaty, Kazakhstan; e-mail: zh.kozhayev@satbayev.university
[5]Bursa Uludag University, Department of Social Studies Education, Bursa, Turkey; e-mail: eatasoy@uludag.edu.tr
[6]Al-Farabi Kazakh National University, Faculty of Geography and Environmental Sciences, Department of Cartography and Geoinformatics, Almaty, Kazakhstan; e-mail: omirzhan.taukebayev@kaznu.edu.kz

Abstract: As a consequence of global population growth and increasing demand for agricultural commodities, vast areas of cultivable land have been brought under cultivation, while natural ecosystems are being converted for agricultural use. This transformation has led to various forms of soil degradation, with excessive salinity emerging as a critical concern. Drought-prone ecosystems are particularly vulnerable to salinization processes, resulting in an annual reduction of arable land by approximately 1% to 2%. In the Kazakhstan, salt-affected soils account for approximately 43% of all agricultural land. The aim of this study is to assess the extent and spatial distribution of soil salinity in the Talas district of Kazakhstan and to identify the dominant chemical characteristics of soil salts across different land types. To achieve this, soil samples were collected from river valleys, desert pastures, irrigated lands, and sandy areas. The analysis focused on salinization processes, ion toxicity thresholds, and the chemical composition of soil salts. Results reveal that salt accumulation varies between the 30 cm and 80 cm soil layers in river valleys and desert pastures, whereas the highest concentrations are observed in the upper layers of irrigated soils. The greatest variation in average salt content by soil texture was ±0.81% in loamy soils and ±0.62% in silty loam soils. These findings highlight the urgent need for ecologically sound land management strategies to mitigate soil salinization, especially in irrigated areas. They also offer

*Corresponding author, e-mail: omirzhan.taukebayev@kaznu.edu.kz

valuable insights for enhancing irrigation efficiency and preserving soil fertility in Talas and other comparable regions.

Keywords: soil salinity; toxic ions; soil texture; landscapes; Talas district (Kazakhstan)

1. Introduction

The global increase in food demand, driven by population growth, has intensified pressure on existing croplands and prompted the expansion of agriculture into natural ecosystems (Fess et al., 2011). This transformation often alters ecological balances, with soil degradation emerging as a critical concern. Among the key drivers of land degradation, soil salinization poses a widespread threat to both natural and cultivated landscapes (Lal, 2012). It is often exacerbated by poor-quality irrigation water, inadequate drainage, monoculture practices, and unsustainable agronomic methods. In arid regions, where soils and groundwater naturally contain elevated salt concentrations, disruption of the hydrological regime can accelerate salinization processes. The resulting salt accumulation significantly undermines soil productivity and ecological resilience (Singh, 2022).

Soil salinization is increasingly recognized as a major global threat due to its detrimental effects on crop productivity, biodiversity, and land sustainability (Gisladottir & Stocking, 2005). Regions such as Africa, South America, and Central and Northern Asia are particularly vulnerable, with saline soils affecting approximately 1,060 million ha as a result of geographic and climatic conditions (Eswar et al., 2021). Variations in soil salinity may arise naturally in arid climates due to irregular precipitation, topography, and soil properties, or be driven by human activities such as over-irrigation, poor drainage, and unsustainable land use (Jones et al., 2012; Shahid et al., 2018). According to FAO estimates from 1988 (as cited in Shahid et al., 2018), approximately 932 million hectares of soils are affected by salinization globally. Various studies, as summarized in the same source, further report that up to 10% of the world's croplands and between 25% and 30% of irrigated lands are impacted by salinity, rendering them significantly less productive and, in some cases, commercially unviable (Shahid et al., 2018). In Kazakhstan, the world's ninth largest country by land area, salinity affects about 43% of agricultural lands (Tokbergenova et al., 2018).

The current distribution of saline soils reflects the complex interplay between natural factors and anthropogenic pressure (Hopmans et al., 2021). For example, the vegetation cover in the Ili delta (Southeastern Kazakhstan) has declined by 12% over the past 40 years, while the share of non-saline soils has decreased by 41.3% due to rising salinity (Laiskhanov et al., 2021). Similar processes have been observed in the Talas valley and delta, which, like the Ili River basin, lie within a temperate desert zone. In such arid landscapes, shifts in water availability whether through climate change or irrigation practices are key drivers of soil salinization and degradation (Curebal et al., 2015; Efe et al., 2012; Laiskhanov et al., 2021). In the Talas district, modeled land cover change from 2000 to 2030 predicts a marked reduction in grasslands (to 334 km^2), a rise in unvegetated lands (up to 2,271 km^2), and the near disappearance of aquatic habitats (reduced to 24 km^2), reflecting widespread ecological transformation (Seitkazy et al., 2024). These changes are accompanied by progressive erosion in the southern parts of the district, a trend expected to continue in future decades (Rakhimova et al., 2024). Salinity dynamics within irrigated areas show clear seasonal fluctuations, particularly during irrigation periods, with deeper soil layers exhibiting higher salt accumulation (Poshanov et al., 2022). Spatial variations in salt distribution correlate with proximity to water bodies and drainage infrastructure (Duan et al., 2022). In southern Kazakhstan, increasing salinization has rendered 236.9 thousand ha (15.2%) of irrigated land unusable (Ministerstvo sel'skogo khozyaistva Respubliki Kazakhstan, 2021). Beyond land use, key factors influencing salinity patterns include soil type, particle-size distribution, and structural attributes such as fractal dimension (Zhao et al., 2016).

Effective agricultural land management and improvements in economic efficiency depend on a clear understanding of the factors limiting soil fertility and the development of evidence-based strategies to address them. Although the importance of monitoring soil salinity across space and time is well established, a critical knowledge gap remains regarding the interaction of key variables shaping salt distribution in soils (Römheld & Kirkby, 2010). This is especially relevant for distinguishing between salinity-induced degradation and land abandonment, both of which carry major implications for land use policy and sustainable development. This study aims to bridge this gap by offering an integrated assessment of spatiotemporal variations in soil salinization and their effects on agricultural productivity. In contrast to earlier approaches, our framework combines spatial assessment with temporal trend analysis to generate actionable insights for managing salinity and promoting sustainable land use under the changing climatic conditions in Talas district (Kazakhstan).

2. Materials and methods

2.1. Study area

The study was conducted in the Talas district of Zhambyl region (42°48'–44°27'N, 69°55'–71°37'E), which covers approximately 12,200 km^2 (Figure 1). The area encompasses the southwestern portion of the arid Moiynkum sandy Desert, the Talas River valley, and adjacent piedmont plains located between the Karatau and Talas Mountain systems. It also includes the intermontane basin and the Aktau Range. The region lies predominantly within the desert zone and is characterized by a sharply continental climate, with cold winters, hot and dry summers, and average annual precipitation ranging between 140 and 230 mm. In the southern mountainous parts, gray and pink soils dominate, while the northern plains are composed of sandy, loamy, and meadow gray soils. The main hydrological axis of the region is the Talas River. The following descriptions of land cover and landscape characteristics rely on the comprehensive data compiled in the National Atlas of the Republic of Kazakhstan (Medeu, 2010).

2.1.1. Land cover and landscapes

The land cover and natural complexes of the study area are primarily shaped by climate. The mountainous zone comprises steppes in low hills and foothills, dominated by gray-chestnut soils, mountain serozems, and crystalline outcrops. Soil formation is most active on slopes, while intermontane valleys feature light northern and meadow serozems.

Vegetation includes montane steppe and friganoid xerophytic communities, rich in endemic species. A characteristic species is *Artemisia karatavica* Krasch. ex Poljakov, thriving in rocky uplands. Friganoid flora includes perennials, semi-shrubs, and shrubs such as *Peganum harmala* L., *Carex pachystylis* Gay, *Artemisia leucodes* Schrenk, *Glycyrrhiza glabra* L., *Salsola arbuscula* Pall., *Cuminum cyminum* L., *Echinops albicaulis* Rgl., and others.

Three main landscape types are observed between the Karatau Mountain system in the north and the Talas River basin in the south. The pre-mountain pediplain, largely underlain by fluvial sediments, includes isolated structural plateaus such as Kyzyltobe. Plains developed under arid conditions are interspersed with meadow soils at elevated sites, while light northern serozems are scattered across the northern sector. The transitional area between lakes Akkol and Ashykol and the Talas valley is characterized by gently undulating terrain with ridges of gravel and coarse sands, supporting sparse woody vegetation. In this zone, limited precipitation and high evapotranspiration restrict soil development and reduce vegetation density. Plant communities here include *Salsola arbusculiformis* Drobov with ephemeral herbs, as well as associations dominated by *Artemisia terrae-albae* Krasch., *Anabasis salsa* (C. A. Mey.) Benth. ex Volkens, *Poa bulbosa* L., *Nanophyton erinaceum* (Pall.) Bunge, and various drought-tolerant *Artemisia* species—*A. semiarida* Krasch., *A. heptapotamica* Poljakov, *A. sublessingiana* (Krasch.) Poljakov—alongside *Stipa sareptana* A. K. Becker and *Stipa richteriana* Kar. & Kir.

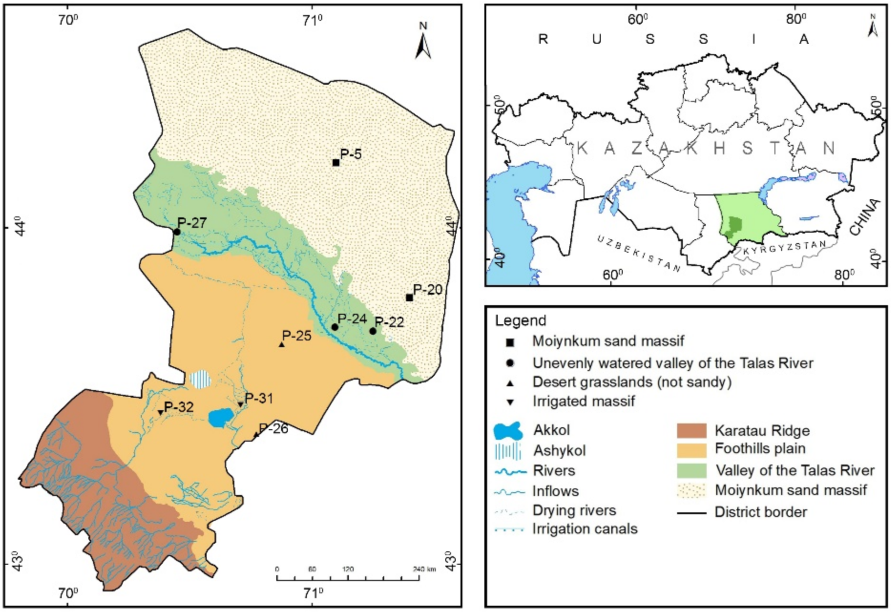

Figure 1. The study area and spatial distribution of sample collection locations.

The Talas River valley is dominated by grey-brown solonchaks and meadow-swamp soils, supporting fragmented tugai (riparian) vegetation. These include tree and shrub species such as *Elaeagnus oxycarpa* Schlecht., *Tamarix ramosissima* Ledeb., *Rosa beggeriana* Schrenk, *Halimodendron halodendron* (Pall.) Voss, and *Clematis orientalis* L.

The Moiynkum Desert represents an arid, sandy landscape where pedogenesis is constrained by limited surface moisture. Sandy substrates are predominant, with isolated occurrences of takir and takir-like soils. Since the Soviet period, afforestation initiatives using saxaul (*Haloxylon* spp.) have been implemented. The sandy terrain supports greater floristic diversity compared to non-sandy desert pastures in the adjacent intermontane plains. Dominant woody species include *Haloxylon persicum* Bunge ex Boiss. & Buhse and *Haloxylon aphyllum* (Minkw.) Iljin, with associated xerophytic taxa such as *Ammodendron bifolium* (Pall.)

Yakovlev, *Calligonum aphyllum* (Pall.) Gürke, tree-like *S. arbuscula* Pall., and *Krasheninnikovia ceratoides* (L.) Gueldenst.

2.2. Data and methods

The Talas district of Zhambyl region (Figure 1) was selected as the study area due to its diverse landscapes and the lack of systematic, science-based field assessments addressing environmental change in recent decades. Fieldwork was conducted four times between 2021 and 2023, during seasons suitable for soil sampling and tracking temporal variations in salinity across soil layers. Given the heterogeneity in salt accumulation across landscape types, vertical soil profiles provide a relevant basis for assessing salinization risks. To date, limited information exists on the geospatial distribution of soil salinity and its environmental implications in the Talas region.

To assess these risks, soil profiles were excavated and morphological descriptions and sampling were conducted following established protocols (Tyurin, 1959). Temporal variation in soil salinity was analyzed using aqueous extract data collected from six depth intervals: 0–5 cm, 10–20 cm, 30–40 cm, 50–60 cm, 70–80 cm, and 90–100 cm. Samples were taken from nine representative sites across four ecosystem types: Moiynkum sands, the Talas River valley, desert grasslands (non-sandy), and irrigated areas. Sampling occurred once in spring 2021, twice in spring and summer 2022, and once in summer 2023.

Salinity was assessed based on chemical composition, degree of salinity, and ion toxicity thresholds. We examined cation (Na^+, K^+, Ca^{2+}, Mg^{2+}) and anion (Cl^-, SO_4^{2+}, HCO_3^-) concentrations in aqueous extracts (He et al., 2012; Mamutov et al., 2011), alongside soil texture was determined according to the United States Department of Agriculture (USDA) texture triangle, based on the relative proportions of sand, silt, and clay (Moreno-Maroto & Alonso-Azcárate, 2022). These parameters serve as effective indicators of salinity level and soil physicochemical properties. Statistical analysis included the Sodium Adsorption Ratio (SAR), calculated using ion concentrations converted to meq/L, according to Equation 1 (Paliwal & Gandhi, 1976):

$$SAR = \frac{N_a{}^+}{\sqrt{\frac{1}{2}(C_a{}^{2+} + M_g{}^{2+})}} \tag{1}$$

Descriptive statistics (mean, median, min–max, and SD) were used to assess the spatial variation in salt content and ion distribution (Mishra et al., 2019). Boxplots were applied to determine ion toxicity thresholds, focusing on central tendency and outliers (Williamson et al., 1989). Piper diagrams were used to visualize major ion chemistry in aqueous extracts, allowing classification of salinity types (e.g., sodium- or calcium-dominant) and facilitating comparative analysis of temporal salt dynamics (He et al., 2021; Wang et al., 2023).

3. Results and discussion

3.1. Textural characteristics of soils and their saline content

Soil structure is a key environmental factor influencing water movement, degradation processes, and soil productivity (Bronick & Lal, 2005). Soil texture in the study area was classified using the USDA texture triangle with samples falling into sand, sandy loam, loam and silty loam categories (Figure 2). The Moiynkum sand complex consists of coarse sandy formations, as exemplified by profiles P-22 and P-31 located in the Talas River valley and irrigated massif. These soils are characterized by large granular particles and wide pore spaces, resulting in high permeability and rapid movement of water and salts (Day, 1956). As a result, average salt concentrations in sand samples remained low, ranging from 0.07% in 2021 to 0.20% in 2023 (Table 1). While sandy soils generally resist salt accumulation under proper drainage conditions, they are vulnerable to salinization in arid climates with high evaporation. Under such conditions, evaporative water loss can draw salt from deeper layers toward the surface (Qi et al., 2002).

Sandy loam, composed primarily of sand with smaller proportions of silt and clay, offers a favorable balance of drainage and water retention, making it well-suited for plant growth and salinity control (Barnard et al., 2010). It represents an intermediate texture between coarse arenaceous and finer loamy soils. In this study, sandy loam horizons were found at 0–20 cm and 0–40 cm depths in profiles P-22 and P-31 from the Talas River valley and irrigated areas (Figure 2). Salt content in sandy loam remained stable in 2021 and 2022 (0.11% and 0.10%, respectively), but increased to 0.24% in spring 2022 and further to 0.66% in 2023, indicating a trend toward salinization (Table 1). Limited water availability or precipitation may restrict leaching, causing salt accumulation in upper layers due to evaporation. This is particularly concerning salt-sensitive crops, as elevated salt concentrations may impair germination and early growth (Rengasamy, 2010). In arid and semi-arid regions, irrigation practices must consider water quality, as mineral-rich water may contribute to salinity if not properly leached (Munns, 2002; Shalhevet, 1994). Compared to pure sand, the finer particles in loam increase water and nutrient retention, but also enhance salt-holding capacity under poor drainage or high evapotranspiration conditions. Effective salinity management requires attention to crop type, irrigation frequency, water quality, climate, and proximity to the water table (Gupta & Huang, 2014).

Loam soil is a well-balanced mixture of sand, silt, and clay, offering several agronomic advantages. This equilibrium contributes to the formation of fertile soils with optimal drainage, adequate aeration, and high nutrient availability. The salinity behavior of loam soil varies depending on multiple factors, including water availability, drainage efficiency, irrigation practices, climatic conditions, and the application of soil amendments and fertilizers. Due to its moderate permeability, loam facilitates the downward movement of water, supporting the leaching of soluble salts and reducing the risk of salt accumulation. However, its response to salinity is not uniform and depends strongly on local hydrological and management conditions (Tang et al., 2020).

Loam soil was primarily found in the topsoil layers of the unevenly irrigated Talas River valley, in the 0–60 cm layers of desert grasslands (excluding sandy zones), and in the deeper horizons (70–80 cm) of irrigated massif profiles (Figure 2). According to statistical data, loam exhibited the highest average salt content among all the textures in the first year (1.03%), with notable seasonal variations in subsequent years: 0.22% in spring and 0.63% in summer of the second year, and 0.46% in the third year (Table 1). These fluctuations reflect the sensitivity of loam to hydrological conditions and management practices. Salinity can increase under restricted water movement caused by high water tables, compaction, or impermeable subsurface layers. Moreover, insufficient rainfall or irrigation may limit leaching, resulting in surface salt accumulation (Beltrán, 1999). In arid zones, poor water quality and high evaporation can exacerbate this effect, causing upward movement of salt-laden water and increasing salinity near the surface (Hillel et al., 2008).

Silt loam, consisting predominantly of silt with smaller amounts of sand and clay, has a smooth texture, high water retention, and enhanced nutrient content compared to sandier soils. Salinity dynamics in this texture are influenced by factors similar to other soil types, such as water availability and drainage (Tang et al., 2020). In this study, silt loam was observed primarily in the Talas River valley, as well as in desert grasslands and irrigated areas. It was most prominent in the lower horizons (10–20 cm) of profiles P-24 and P-26, the entirety of profile P-27, and in the 0–60 cm depth of profile P-32 (Figure 2). These soils lacked sandy components. Salt accumulation patterns in silt loam varied over time (Table 1): the mean concentration was 0.65% in summer 2021, increased to 0.93% in spring 2022, then declined to 0.36% in summer 2022 and 0.31% in summer 2023. These fluctuations suggest sensitivity to seasonal hydrological conditions and soil profile structure.

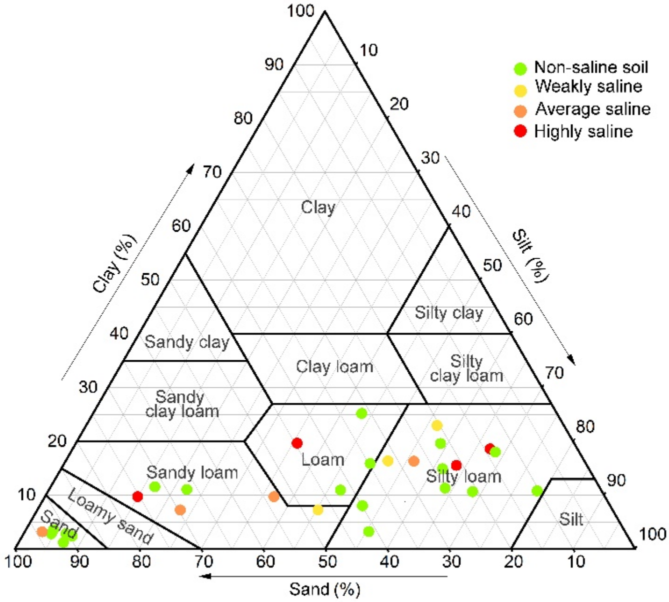

Figure 2. Soil texture triangle showing classified samples (salinity levels) from Talas district ecosystems.

Silt loam is well known for its strong water retention and favorable drainage properties, which help reduce waterlogging and lower the risk of salinization. However, if drainage is impeded—due to a high water table, a hardpan layer, or other limiting conditions—the leaching of soluble salts may be restricted, contributing to increased surface salinity (Zia-ur-Rehman et al., 2016). Moreover, because of its fine particle size, silt loam is susceptible to surface crust formation, which decreases water infiltration and enhances salt accumulation through evaporation (Minhas et al., 1986).

The granulometric composition of soil samples from the study area was classified using the USDA textural system, which grouped them into sand, sandy loam, loam, and silty loam textures (Moreno-Maroto & Alonso-Azcárate, 2022). Notable variation in total salt content was observed, with temporal fluctuations and pronounced differences between minimum and maximum salinity values across textures. The most frequently identified types were sandy loam, loam, and silt loam. The widest disparity occurred in spring 2022, ranging from 0.11% to 2.94% in silt loam, 0.11% to 2.35% in loam (summer 2021), and 0.11% to 1.58% in sandy loam. A distinct increase was recorded in sandy soils in summer 2023, peaking at 0.80%, likely due to the 50–60 cm horizon of profile P-31 within the irrigated massif (Table 1). As a result, the average salt level in this profile exceeded other textures, indicating a notable influence. The arithmetic mean, calculated as the sum of all values divided by the number of samples, reflects general salinity trends, but is sensitive to outliers that may distort interpretation (Williamson et al., 1989). Salinity variation is strongly affected by soil texture, which governs drainage, water retention, cation exchange, and evaporation. Thus, effective salinity management requires texture-specific strategies adapted to each soil type (Hopmans et al., 2021).

Table 1. Statistical results of the sum of salts in soil structure parameters (sum of salts in % of per 100 grams' dry soil)

Parameters	Sampling time	Mean	Minimum	Maximum	Median	SD
Sand	Summer, 2021	0.07	0.04	0.14	0.06	0.04
	Spring, 2022	0.05	0.03	0.08	0.04	0.02
	Summer, 2022	0.14	0.03	0.37	0.05	0.15
	Summer, 2023	0.20	0.03	0.80	0.05	0.30
Sandy loam	Summer, 2021	0.11	0.11	0.13	0.11	0.01
	Spring, 2022	0.10	0.05	0.16	0.09	0.04
	Summer, 2022	0.24	0.09	0.48	0.17	0.17
	Summer, 2023	0.66	0.11	1.58	0.52	0.62
Loam	Summer, 2021	1.03	0.11	2.35	0.77	1.00
	Spring, 2022	0.22	0.04	0.80	0.09	0.32
	Summer, 2022	0.63	0.07	1.82	0.50	0.71
	Summer, 2023	0.46	0.10	1.54	0.18	0.61
Silt loam	Summer, 2021	0.65	0.05	1.11	0.74	0.39
	Spring, 2022	0.93	0.11	2.94	0.75	0.99
	Summer, 2022	0.36	0.05	0.81	0.14	0.35
	Summer, 2023	0.31	0.06	1.33	0.16	0.37

3.2. The dynamics and classification of soil salinization

The total salt content and its variability in soils can differ considerably depending on land use and ecosystem characteristics (Pouyat et al., 2007). Soil salinity is influenced by climatic conditions (humidity, evaporation, precipitation), groundwater depth, soil texture, vegetation cover, and anthropogenic factors. Salinity levels vary both spatially and temporally (Hopmans et al., 2021). Salinity assessment typically involves analyzing aqueous extracts from soil samples to determine water-extractable salt concentrations at various depths. This widely used method effectively quantifies salt content across soil profiles. For each sample, 100 g of dry soil were used, and classification was based on the criteria in Table 2, which defines salinity levels by percentage of total salts relative to dry mass (Mamutov et al., 2011). Salinity patterns in the study area exhibited seasonal and interannual fluctuations. In summer 2021, 59.3% of samples were non-saline. This proportion increased to 70.4% in spring 2022, then decreased to 52.6% in summer 2022, and rose again to 63.0% in summer 2023. Between spring and summer 2022, the share of non-saline soil dropped by 17.8%. Weakly saline soil was absent in summer 2021, but appeared in 3.7% of samples in spring 2022, increasing to 15.8% in summer 2022, then falling to 7.4% in 2023. The proportion of weakly saline soils has increased compared to the first year. Average saline soils accounted for 25.9% and 26.3% in summers of 2021 and 2022, and 14.8% in both spring and summer 2022. Highly saline soils were observed in 14.8% of samples in spring 2021, 11.1% in both spring 2022 and summer 2023, and 5.3% in summer 2022. Overall, the trend suggests an increase in non-saline and weakly saline soils, with fluctuating levels in other salinity categories (Table 2).

Table 2. Categorization of soil saline levels and proportional distribution of soil samples across study periods

Total salt content (%)	Salinity classification	Sampling time			
		Summer, 2021	Spring, 2022	Summer, 2022	Summer, 2023
< 0.25	Non-saline soil	59.3	70.4	52.6	63.0
0.25–0.5	Weakly saline	0	3.7	15.8	7.4
0.5–1.0	Average saline	25.9	14.8	26.3	14.8
> 1	Highly saline	14.8	11.1	5.3	11.1

To visualize the distribution of soil salinity and ion toxicity across layers, boxplots were used as a statistical tool (Figure 3 and Figure 4). The *x*-axis represents sampling periods across four ecosystem types—Moiynkum sands, the unevenly watered Talas River valley, desert grasslands, and irrigated massifs—during summer 2021, spring and summer 2022, and summer 2023. The *y*-axis displays salinity levels derived from aqueous extracts (expressed in % or mg-eq per 100 g of soil). Each box represents the interquartile range (25th–75th percentiles), with the internal line showing the median and a star symbol indicating the mean.

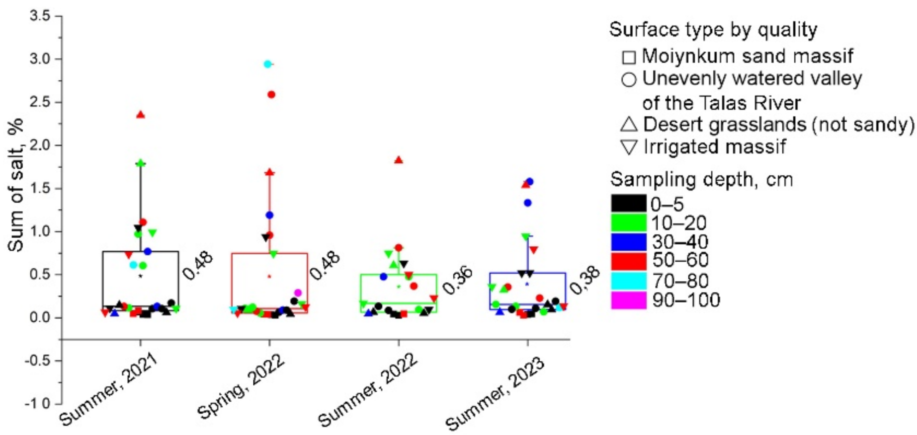

Figure 3. Box plot of the sum of salt for samples taken from different sites and at different times.

In all the sampling periods, mean values exceeded those of non-saline soils and fell within the weakly saline category. Whiskers extend to indicate the data range, highlighting both distribution and potential outliers. This visualization allowed us to identify the depth and period of peak salt accumulation and ion variability across profiles. According to total salt content (Figure 3), highly saline soils were observed in summer 2021 at 0–20 cm and 50–60 cm depths in the desert grassland, 50–60 cm in the Talas River valley, and 0–5 cm and 10–20 cm in irrigated massifs. In contrast, in spring 2022, the Talas valley exhibited increased salinity at 30–40 cm, 50–60 cm, and 70–80 cm depths, while the desert grassland showed reduced salinity limited to the 50–60 cm layer. In irrigated massifs, areas previously classified as highly saline transitioned to moderately saline levels. During summers 2022 and 2023, highly saline zones diminished, while weakly and moderately saline soils became more common, as reflected by the broader interquartile spread in the boxplots. Notably, the greatest salinity variation occurred in the 10–20 cm and 50–60 cm layers of desert grasslands, whereas the 0–5 cm layers showed the lowest variation across both the Talas valley and irrigated zones. Surface layers in irrigated massifs (0–5 cm and 10–20 cm) remained primarily in the weakly to moderately saline range with minimal variability.

3.3. Chemical properties of sampling soils

Although often conflated, salinity and sodicity are distinct. Sodicity refers specifically to elevated sodium concentrations, whereas salinity encompasses a broader spectrum of soluble salts, including sodium, calcium, magnesium, chloride, sulfate, and carbonates/bicarbonates. The potential impacts of high concentrations of individual ions depend on plant or microbial sensitivity, climate, and soil properties (Munns & Tester, 2008). Nonetheless, established toxicity thresholds for certain ions in milliequivalents per 100 g of soil are as follows: carbonate (CO_3^{2-}) – 0.03; bicarbonate (HCO_3^-) – 0.8; chloride (Cl^-) – 0.3; sulfate (SO_4^{2-}) – 1.7 (Mamutov et al., 2011). To assess ion-specific toxicity levels and their influence on salinity variability, we applied boxplot analysis (Figure 4).

In the first year, CO_3^{2-} concentrations were generally low, clustered within the 50th percentile. However, elevated values were detected at 10–20 cm, 50–60 cm, and 70–80 cm depths in irrigated massif profiles, and at 30–60 cm layers in the unevenly watered Talas River valley, indicating localized exceedances of the toxicity threshold. By 2022–2023, carbonate distribution became more variable, particularly in irrigated zones and deeper desert grassland layers, whereas surface layers (0–5 cm) remained low. Carbonates typically occur as calcium carbonate (lime), which may buffer soil acidity. Yet under arid conditions, excessive carbonate can lead to calcic horizon development (hardpans), restricting root penetration. Additionally, under highly alkaline conditions (pH > 8.5), the availability of key micronutrients may decline significantly (Doner & Grossl, 2002). HCO_3^- is commonly associated with alkaline and saline soils. At elevated concentrations, it can induce iron chlorosis in plants by reducing the availability of iron and other micronutrients. As shown in Figure 4, abnormal values were recorded in irrigated field samples at 0–20 cm and 50–80 cm, with most exceeding the toxicity threshold of 0.8 meq/100 g. In contrast, bicarbonate levels in other ecosystems generally remained below this limit. In spring of the second year, bicarbonate concentrations declined in lower soil horizons, while topsoil values increased. By summer, desert grassland samples showed sharp rises at 10–20 cm and 50–60 cm. In the third year, the highest concentrations were observed again in the sand grassland and irrigated massifs. Other ecosystems remained within safe levels. Cl^- is a soluble salt that induces osmotic stress, reducing plants' water uptake even when water is available. High chloride levels can also cause direct toxicity, such as leaf burns and growth suppression (Nemati et al., 2011). Across all sampling periods, mean Cl^- concentrations exceeded the toxicity threshold, particularly in the Talas River valley, desert grasslands, and irrigated areas. Notably, high chloride levels were found mainly in the arable layers of irrigated soils; in other ecosystems, surface horizons remained below the threshold. Elevated chloride was consistently found at 10–20 cm, 30–40 cm, and 50–60 cm depths (Figure 4).

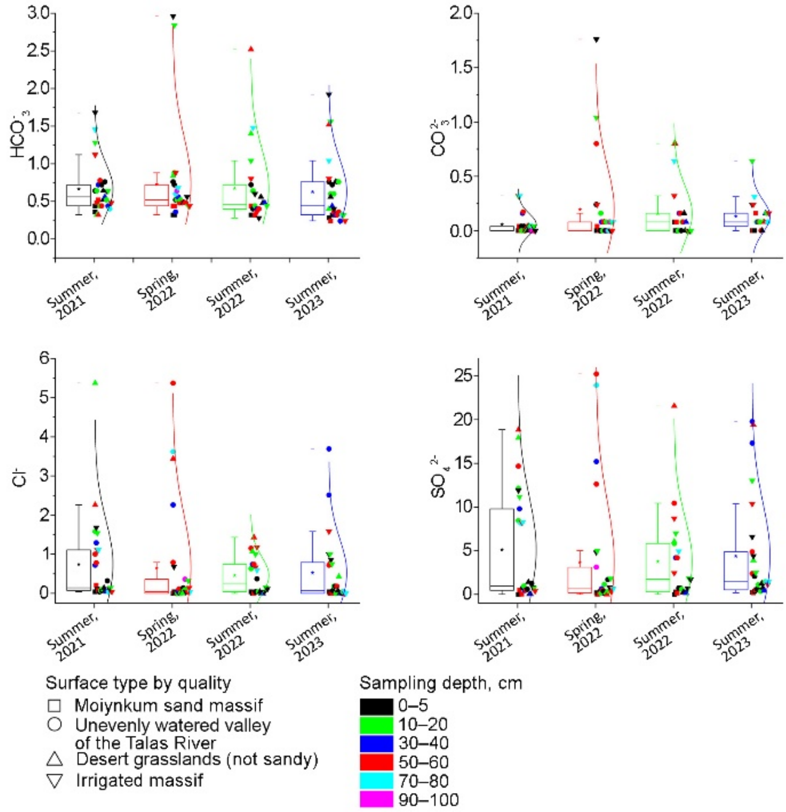

Figure 4. Box plot presenting specific ions for samples taken from different landscape types and by seasons.

SO_4^{2-} plays an essential role in plant metabolism, contributing to amino acid and protein synthesis (Ali et al., 2018; Munns & Tester, 2008). However, excessive sulfate, especially when associated with low pH, may lead to structural soil degradation and nutrient leaching, ultimately reducing yields (Yadav et al., 2020). In this study, sulfate exceeded the toxicity threshold mainly in desert grassland soils (10–60 cm), the Talas River valley, and surface layers of irrigated massifs. In the second year, elevated sulfate was observed only in the Talas valley. During the summers of 2022 and 2023, most samples above the limit came from this ecosystem.

The boxplot analysis (Figure 4) provided an integrated overview of salt distribution by depth and ecosystem, revealing both variability and outliers. It allowed for the identification of horizons most at risk for ion-specific toxicity, aiding in the development of targeted soil management strategies.

Understanding the ecological impact of saline soils requires examining their chemical composition first. Saline soils contain a variety of salts, including sodium chloride (NaCl), magnesium chloride ($MgCl_2$), calcium chloride ($CaCl_2$), magnesium sulfate ($MgSO_4$), and sodium sulfate (Na_2SO_4), among others. These salts originate from multiple sources such as weathering of parent rock material, saline irrigation water, or upward capillary movement from a high water table (Richards, 1954). To assess soil salinity composition, we employed Piper diagrams, a trilinear graphical tool used to classify water and soil based on dominant ions (Piper, 1944). The diagram organizes major cations (Na^+, K^+, Ca^{2+}, Mg^{2+}) and anions (SO_4^{2-}, HCO_3^-, Cl^-) into a compositional matrix that helps visualize and interpret ionic dominance patterns. Piper plots do not typically account for trace elements or minor ions. Based on this analysis, the soil samples in our study area were classified into three primary salinity types: magnesium bicarbonate, mixed Ca-Mg-Cl, and sodium chloride (Figure 5).

As the name implies, this soil type is dominated by magnesium and bicarbonate ions. On the Piper diagram, such samples plot toward the lower left corner of the cation triangle, indicating magnesium dominance. These soils were initially identified in 2021 in surface horizons (0–5 cm) from the Moiynkum sand Massif, the 10–20 cm layer of the unevenly irrigated Talas River valley, and the 30–40 cm depth in the desert grassland. In subsequent campaigns, magnesium-bicarbonate profiles were found in the 50–60 cm horizon in spring and 0–5 cm layer in summer, both from the Moiynkum Massif. By the third year, samples from 10–20 cm depth in the irrigated massif also fell into this category. In the central diamond field of the Piper diagram, these samples clustered in the upper-left quadrant, combining surface soils from Moiynkum with fluvial terrace profiles from Talas River sites. High bicarbonate levels in these soils are likely associated with mineral dissolution or organic matter decomposition. In the anion triangle, all related samples plotted within the bicarbonate and sulfate regions (lower left and upper fields, respectively) (Figure 5).

Mixed-type soils exhibit no clear dominance of a single cation or anion, often plotting variably within the central diamond field of the Piper diagram. This heterogeneity results from overlapping processes such as evaporation, dilution, ion exchange, and mineral weathering. Their ambiguous chemical profile necessitates careful management to avoid fertility imbalances, structural instability, and water retention issues. In our study, approximately half of the samples analyzed consistently occupied this transitional region. Sodium–chloride-type soils, by contrast, are classically saline due to elevated Na^+ and Cl^- concentrations. On the Piper diagram, they cluster toward the sodium-dominated corner of the cation triangle and appear in the lower left quadrant of the diamond field. In our observations, all sampling sites—except those within the Moiynkum sand Massif—NaCl-type profiles at some stage. These samples were predominantly collected from middle and lower horizons, where high salt accumulation was most evident. Such soil poses agronomic and ecological challenges, including disrupted plant uptake and compromised soil structure. Moreover, temporal shifts were observed in the positioning of chemical types: by summer 2023, several profiles transitioned from bicarbonate-dominant to strong-acid (Cl^-, SO_4^{2-}) dominant types, indicating progressive salinization and changing ion composition.

Sodic soils, characterized by high concentrations of Na^+ and HCO_3^-/CO_3^{2-}, typically exhibit elevated SAR values. However, such soils were not identified among our samples analyzed. SAR was calculated using the standard formula provided earlier to assess the degree of sodicity. Although no soils met the criteria for sodic classification, elevated SAR values were observed in the middle and lower horizons of profiles P-25, P-27, and P-32, suggesting localized sodium accumulation without exceeding sodicity thresholds.

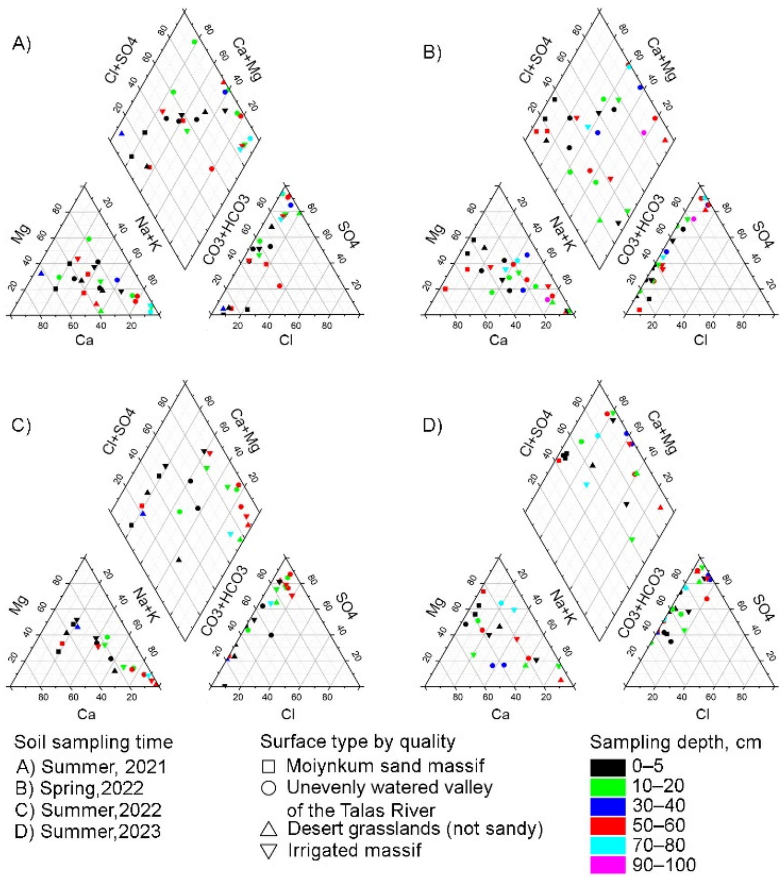

Figure 5. Piper diagram presenting the distribution of anionic and cationic compositions of the soils.

The vertical distribution of soluble salts within a soil profile offers key insight into salinization dynamics. Using profile P-27 as a representative example, we visualized ion concentrations across depth and time (Figure 6). The profile includes three graphs from the same location across different sampling periods. In 2021, the salt content varied by depth, with relatively moderate concentrations. By the second year, ion accumulation became more pronounced in deeper horizons. In the third year, peak concentrations were observed at 30–40 cm, indicating mid-profile salt accumulation. These subsurface layers, though less affected by surface disturbances, may accumulate salt due to capillary rise from saline groundwater or due to inherited geochemical conditions. This underscores the importance of monitoring not only surface salinity but also vertical movement of salts within soil profiles.

Quantitative assessment of soil salinity in the study area reveals pronounced salt enrichment in surface horizons, particularly in irrigated zones where carbonate and bicarbonate ions dominate. This pattern is strongly influenced by the mineralization of river water, especially in floodplain meadow soils. The northern and central parts of the region lie within the Talas River basin, including its delta zone, which is characterized by a calm hydrological regime. During the irrigation season, flooding may occur depending on discharge volumes. In contrast, the southern sector belongs to the catchments of smaller rivers—such as the Assy and Koktal—originating from the northeastern slopes of the Karatau Range. These streams are highly dependent on winter precipitation, with the lowest water levels recorded in late summer.

The mineralization of river water in the region is shaped by the hydrological regime, lithological background, temperature fluctuations (particularly in summer), drainage and industrial discharge (Burlybaev et al., 2018). The Talas River exhibits a bicarbonate-calcium composition, with minimal mineralization (73.9–270.6 mg/dm^3) during spring floods, and elevated values (127.9–438.1 mg/dm^3) in late summer and winter due to dominant groundwater input. During these low-flow periods, water chemistry is typically dominated by HCO_3^- (28.9–46.4%) and Ca^{2+} (21.7–40.2%).

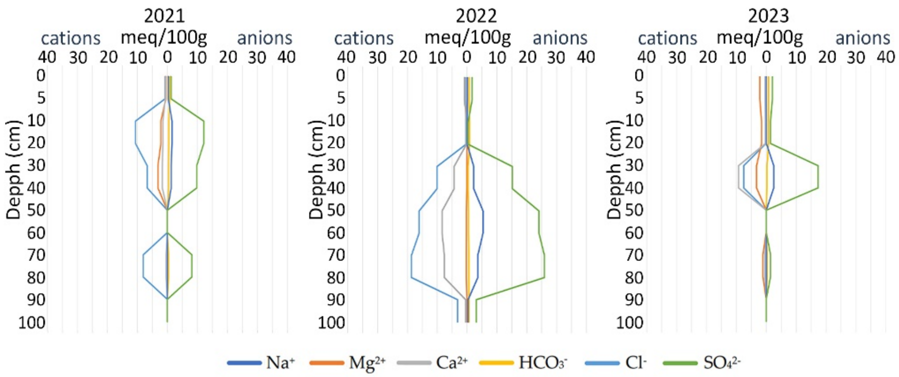

Figure 6. Salt profile presenting variability of the anionic and cationic compositions in the total amount of salt (P-27).

Salt redistribution in soil is influenced by evaporation and infiltration cycles, especially in arid environments. In dry periods, surface evaporation concentrates salt in upper layers, while rainfall and irrigation subsequently washes ions downward, leading to subsoil accumulation. Inherited geological salinity also contributes to this vertical transport of salts. In spring 2022, a temporal decline in surface salinity was observed, while deeper layers in the Talas River valley, desert grasslands, and irrigated massifs showed progressive salt buildup. These patterns reflect the region's arid climate, limited precipitation, and high evaporation rates.

The granulometric composition of soils—proportions of sand, silt, and clay—affects salinity by influencing water retention, permeability, and erosion potential (Li et al., 2014). Salt accumulation patterns varied significantly by texture, with the widest fluctuation in loam soils (±0.81%), followed by silt loam (±0.62%), indicating that loamy soils are more prone to salinity variation. These results underscore the importance of soil texture in assessing and managing salinization processes.

4. Conclusion

This study highlights the practical implications of analyzing the geospatial and temporal dynamics of soil salinity for sustainable land management. Results from 2021 to 2023 reveal a progressive increase in total salinity and ion concentrations, largely influenced by soil texture, local ecosystems, and land use practices. The observed salinization poses a serious threat to ecosystems, degrades soil quality, and reduces agricultural productivity, particularly in irrigated zones and areas near rivers or lakes. As salinity continues to expand due to limited water availability and inadequate management, the risk of land abandonment increases. These findings underscore the urgency of adopting integrated strategies to monitor, mitigate, and manage salinity. Future research should focus on identifying at-risk zones and supporting long-term agricultural sustainability through targeted remediation and soil conservation practices.

Acknowledgements

This research is funded by the Science Committee of the Ministry of Science and Higher Education of the Republic of Kazakhstan (Grant No. AP09058590).

References

Ali, A. S., Hassan, A. M., Saber, N. E., & Elhosary, E. G. (2018). Role of sulphate (SO_4^{2-}) in improvement the growth of rocket plants (*Eruca sativa* L.) under selenate (SeO_4^{2-}) levels. *Plant Omics*, *11*(1), 50–57. https://search.informit.org/doi/10.3316/informit.538895552765123

Barnard, J. H., van Rensburg, L. D., & Bennie, A. T. P. (2010). Leaching irrigated saline sandy to sandy loam apedal soils with water of a constant salinity. *Irrigation Science*, *28*, 191–201. https://doi.org/10.1007/s00271-009-0175-y

Beltrán, J. M. (1999). Irrigation with saline water: benefits and environmental impact. *Agricultural Water Management*, *40*(2–3), 183–194. https://doi.org/10.1016/S0378-3774(98)00120-6

Bronick, C. J., & Lal, R. (2005). Soil structure and management: a review. *Geoderma*, *124*(1–2), 3–22. https://doi.org/10.1016/j.geoderma.2004.03.005

Burlybaev, M. Zh., Shenberger, I. V., Burlybaeva, D. M., Smirnova, D. A., Sokolskii, V. A., Aytureev, A. M., Linnik, A. S., & Milyukov, D. Yu. (2018). *Problemy zagryazneniya osnovnykh transgranichnykh rek Kazakhstana. Tom 3: Basseiny rek Shu i Talas* [Problems of pollution of major transboundary rivers of Kazakhstan. Vol. 3: Basins of the Shu and Talas Rivers]. Kaganat Publishing.

Curebal, I., Efe, R., Soykan, A., & Sonmez, S. (2015). Impacts of anthropogenic factors on land degradation during the anthropocene in Turkey. *Journal of Environmental Biology*, *36*, 51–58. https://pubmed.ncbi.nlm.nih.gov/26591882/

Day, P. R. (1956). Dispersion of a moving salt-water boundary advancing through saturated sand. *Eos, Transactions American Geophysical Union*, *37*(5), 595–601. https://doi.org/10.1029/TR037i005p00595

Doner, H. E., & Grossl, P. R. (2002). Carbonates and Evaporites. In J. B. Dixon & D. G. Schulze (Eds.), *Soil Mineralogy with Environmental Applications* (pp. 199–228). Soil Science Society of America, Inc. https://doi.org/10.2136/sssabookser7.c6

Duan, Y., Ma, L., Abuduwaili, J., Liu, W., Saparov, G., & Smanov, Z. (2022). Driving Factor Identification for the Spatial Distribution of Soil Salinity in the Irrigation Area of the Syr Darya River, Kazakhstan. *Agronomy*, *12*(8), Article 1912. https://doi.org/10.3390/agronomy12081912

Efe, R., Soykan, A., Curebal, I., & Sonmez, S. (2012). Land use and land cover change detection in Karinca river catchment (NW Turkey) using GIS and RS techniques. *Journal of Environmental Biology*, *33*, 439–447. http://www.jeb.co.in/journal_issues/201204_apr12_supp/paper_20.pdf

Eswar, D., Karuppusamy, R., & Chellamuthu, S. (2021). Drivers of soil salinity and their correlation with climate change. *Current Opinion in Environmental Sustainability*, *50*, 310–318. https://doi.org/10.1016/j.cosust.2020.10.015

Fess, T. L., Kotcon, J. B., & Benedito, V. A. (2011). Crop Breeding for Low Input Agriculture: A Sustainable Response to Feed a Growing World Population. *Sustainability, 3*(10), 1742–1772. https://doi.org/10.3390/su3101742

Gisladottir, G., & Stocking, M. (2005). Land degradation control and its global environmental benefits. *Land Degradation & Development, 16*(2), 99–112. https://doi.org/10.1002/ldr.687

Gupta, B., & Huang, B. (2014). Mechanism of Salinity Tolerance in Plants: Physiological, Biochemical, and Molecular Characterization. *International Journal of Genomics*, *2014*(1), Article 701596. https://doi.org/10.1155/2014/701596

He, J., Den, Q., Ma, X., Su, X., & Ma, X. (2021). Soil salinization affected by hydrogeochemical processes of shallow groundwater in Cangzhou City, a coastal region in North China. *Hydrology Research*, *52*(5), 1116–1131. https://doi.org/10.2166/nh.2021.183

He, Y., DeSutter, T., Prunty, L., Hopkins, D., Jia, X., & Wysocki, D. A. (2012). Evaluation of 1:5 soil to water extract electrical conductivity methods. *Geoderma*, *185–186*, 12–17. https://doi.org/10.1016/j.geoderma.2012.03.022

Hillel, D., Braimoh, A. K., & Vlek, P. L. G. (2008). Soil Degradation Under Irrigation. In A. K. Braimoh & P. L. G. Vlek (Eds.), *Land Use and Soil Resources* (pp. 101–119). Springer. https://doi.org/10.1007/978-1-4020-6778-5_6

Hopmans, J. W., Qureshi, A. S., Kisekka, I., Munns, R., Grattan, S. R., Rengasamy, P., Ben-Gal, A., Assouline, S., Javaux, M., Minhas, P. S., Raats, P. A. C., Skaggs, T. H., Wang, G., De Jong van Lier, Q., Jiao, H., Lavado, R. S., Lazarovitch, N., Li, B., & Taleisnik, E. (2021). Critical knowledge gaps and research priorities in global soil salinity. In D. L. Sparks (Ed.), *Advances in Agronomy* (pp. 1–191). https://doi.org/10.1016/bs.agron.2021.03.001

Jones, A., Panagos, P., Barcelo, S., Bouraoui, F., Bosco, C., Dewitte, O., Gardi, C., Erhard, M., Hervás, J., Hiederer, R., Jeffery, S., Lükewille, A., Marmo, L., Montanarella, L., Olazábal, C., Petersen, J.-E., Penizek, V., Strassburger, T., Tóth, G., . . . Yigini, Y. (2012). *The State of Soil in Europe – A contribution of the JRC to the European Environment Agency's Environment State and Outlook Report—SOER 2010*. Publications Office of the European Union. https://core.ac.uk/reader/38625630

Laiskhanov, S. U., Poshanov, M. N., Smanov, Z. M., Karmenova, N. N., Tleubergenova, K. A., & Ashimov, T. A. (2021). A Study of the Processes of Desertification at the Modern Delta of the Ili River with the Application of Remote Sensing Data. *Journal of Ecological Engineering, 22*(3), 169–178. https://doi.org/10.12911/22998993/132546

Lal, R. (2012). Climate Change and Soil Degradation Mitigation by Sustainable Management of Soils and Other Natural Resources. *Agricultural Research, 1*, 199–212. https://doi.org/10.1007/s40003-012-0031-9

Li, X., Chang, S. X., & Salifu, K. F. (2014). Soil texture and layering effects on water and salt dynamics in the presence of a water table: a review. *Environmental Reviews, 22*(1), 41–50. https://doi.org/10.1139/er-2013-0035

Mamutov, Z. U., Mamontov, V. G., & Esimbekov, M. B. (2011). *Interpretation of the data of the aqueous extract from saline soils*. Polygraphy–Service K.

Medeu, A. R. (Ed.). (2010). *National Atlas of the Republic of Kazakhstan. Vol. 1: Natural Conditions and Resources* (2nd ed.). Institute of Geography, National Scientific and Technological Holding "Parasat".

Minhas, P. S., Khosla, B. K., & Prihar, S. S. (1986). Evaporation and redistribution of salts in a silt loam soil as affected by tillage induced soil mulch. *Soil and Tillage Research, 7*(4), 301–313. https://doi.org/10.1016/0167-1987(86)90018-8

Ministerstvo sel'skogo khozyaistva Respubliki Kazakhstan. (2021). *Svodnyi analiticheskii otchet o sostoyanii i ispol'zovanii zemel' Respubliki Kazakhstan za 2020 god* [Summary analytical report on the state and use of land in the Republic of Kazakhstan for 2020]. Ministry of Agriculture of the Republic of Kazakhstan. https://www.gov.kz/memleket/entities/land/documents/details/126567?lang=ru

Mishra, P., Pandey, C. M., Singh, U., Gupta, A., Sahu, C., & Keshri, A. (2019). Descriptive Statistics and Normality Tests for Statistical Data. *Annals of Cardiac Anaesthesia, 22*(1), 67–72. https://doi.org/10.4103/aca.ACA_157_18

Moreno-Maroto, J. M., & Alonso-Azcárate, J. (2022). Evaluation of the USDA soil texture triangle through Atterberg limits and an alternative classification system. *Applied Clay Science*, *229*, Article 106689. https://doi.org/10.1016/j.clay.2022.106689

Munns, R. (2002). Comparative physiology of salt and water stress. *Plant, Cell & Environment*, *25*(2), 239–250. https://doi.org/10.1046/j.0016-8025.2001.00808.x

Munns, R., & Tester, M. (2008). Mechanisms of Salinity Tolerance. *Annual Review of Plant Biology*, *59*, 651–681. https://doi.org/10.1146/annurev.arplant.59.032607.092911

Nemati, I., Moradi, F., Gholizadeh, S., Esmaeili, M. A., & Bihamta, M. R. (2011). The effect of salinity stress on ions and soluble sugars distribution in leaves, leaf sheaths and roots of rice (*Oryza sativa* L.) seedlings. *Plant, Soil and Environment, 57*(1), 26–33. https://doi.org/10.17221/71/2010-PSE

Paliwal, K. V., & Gandhi, A. P. (1976). Effect of salinity, SAR, Ca:Mg ratio in irrigation water, and soil texture on the predictability of exchangeable sodium percentage. *Soil Science*, *122*(2), 85–90. https://journals.lww.com/soilsci/abstract/1976/08000/EFFECT_OF_SALINITY,_SAR,_Ca__Mg_RATIO_IN.4.aspx

Piper, A. M. (1944). A graphic procedure in the geochemical interpretation of water-analyses. *Eos, Transactions American Geophysical Union*, *25*(6), 914–928. http://dx.doi.org/10.1029/TR025i006p00914

Poshanov, M. N., Laiskhanov, S. U., Smanov, Z. M., Kenenbayev, S. B., Aliaskarov, D. T., Abikbayev, Y. R., Vyrakhmanova, A. S., & Askanbek, A. (2022). The Effects of the Degree of Soil Salinity and the Bio preparation on Productivity of Maize in the Shaulder Irrigated Massif. *OnLine Journal of Biological Sciences*, *22*(1), 58–67. https://doi.org/10.3844/ojbsci.2022.58.67

Pouyat, R. V., Yesilonis, I. D., Russell-Anelli, J., & Neerchal, N. K. (2007). Soil Chemical and Physical Properties That Differentiate Urban Land-Use and Cover Types. *Soil Science Society of America Journal, 71*(3), 1010–1019. https://doi.org/10.2136/sssaj2006.0164

Qi, F., Kunihiko, E., & Guodong, C. (2002). Soil water and chemical characteristics of sandy soils and their significance to land reclamation. *Journal of Arid Environments, 51*(1), 35–54. https://doi.org/10.1006/jare.2001.0928

Rakhimova, M., Zulpykharov, K., Assylbekova, A., Zhengissova, N., & Taukebayev, O. (2024). Using the Revised Universal Soil Loss Equation and Global Climate Models (CMIP6) to Predict Potential Soil Erosion Associated with Climate Change in the Talas District, Kazakhstan. *Sustainability*, *16*(2), Article 574. https://doi.org/10.3390/su16020574

Rengasamy, P. (2010). Soil processes affecting crop production in salt-affected soils. *Functional Plant Biology, 37*(7), 613–620. https://doi.org/10.1071/FP09249

Richards, L. A. (Ed.). (1954). *Diagnosis and Improvement of Saline and Alkali Soils*. United States Department of Agriculture.

Römheld, V., & Kirkby, E. A. (2010). Research on potassium in agriculture: needs and prospects. *Plant and Soil, 335*, 155–180. https://doi.org/10.1007/s11104-010-0520-1

Seitkazy, M., Beisekenov, N., Taukebayev, O., Zulpykharov, K., Tokbergenova, A., Duisenbayev, S., Sarybaev, E., & Turymtayev, Z. (2024). Forecasting Land Use Dynamics in Talas District, Kazakhstan, Using Landsat Data and the Google Earth Engine (GEE) Platform. *Sustainability*, *16*(14), Article 6144. https://doi.org/10.3390/su16146144

Shahid, S. A., Zaman, M., & Heng, L. (2018). Soil Salinity: Historical Perspectives and a World Overview of the Problem. In *Guideline for Salinity Assessment, Mitigation and Adaptation Using Nuclear and Related Techniques* (pp. 43–53). Springer. https://doi.org/10.1007/978-3-319-96190-3_2

Shalhevet, J. (1994). Using water of marginal quality for crop production: major issues. *Agricultural Water Management*, *25*(3), 233–269. https://doi.org/10.1016/0378-3774(94)90063-9

Singh, A. (2022). Soil salinity: A global threat to sustainable development. *Soil Use and Management, 38*(1), 39–67. https://doi.org/10.1111/sum.12772

Tang, S., She, D., & Wang, H. (2020). Effect of salinity on soil structure and soil hydraulic characteristics. *Canadian Journal of Soil Science, 101*(1), 62–73. https://doi.org/10.1139/cjss-2020-0018

Tokbergenova, A., Kiyassova, L., & Kairova, S. (2018). Sustainable Development Agriculture in the Republic of Kazakhstan. *Polish Journal of Environmental Studies*, *27*(5), 1923–1933. https://doi.org/10.15244/pjoes/78617

Tyurin, I. V. (1959). Methods and techniques of field soil survey. In *Soil Survey: A Guide to Field Investigations and Mapping of Soils* (pp. 44–104). Academy of Sciences of the USSR.

Wang, D., Zhang, L., Zhang, J., Li, W., Li, H., Liang, Y., Han, Y., Luo, P., & Wang, Z. (2023). Effect of Magnetized Brackish Water Drip Irrigation on Water and Salt Transport Characteristics of Sandy Soil in Southern Xinjiang, China. *Water, 15*(3), Article 577. https://doi.org/10.3390/w15030577

Williamson, D. F., Parker, R. A., & Kendrick, J. S. (1989). The Box Plot: A Simple Visual Method to Interpret Data. *Annals of Internal Medicine*, *110*(11), 916–921. https://doi.org/10.7326/0003-4819-110-11-916

Yadav, D. S., Jaiswal, B., Gautam, M., & Agrawal, M. (2020). Soil Acidification and its Impact on Plants. In P. Singh, S. K. Singh, & S. M. Prasad (Eds.), *Plant Responses to Soil Pollution* (pp. 1–26). Springer. https://doi.org/10.1007/978-981-15-4964-9_1

Zhao, Y., Feng, Q., & Yang, H. (2016). Soil salinity distribution and its relationship with soil particle size in the lower reaches of Heihe River, Northwestern China. *Environmental Earth Sciences*, *75*, Article 810. https://doi.org/10.1007/s12665-016-5603-8

Zia-ur-Rehman, M., Murtaza, G., Qayyum, M. F., Saifullah, Rizwan, M., Ali, S., Akmal, F., & Khalid, H. (2016). Degraded Soils: Origin, Types and Management. In K. R. Hakeem, J. Akhtar, & M. Sabir (Eds.), *Soil Science: Agricultural and Environmental Prospectives* (pp. 23–65). Springer. https://doi.org/10.1007/978-3-319-34451-5_2